Carrier transport in nanoporous TiO_2 films

R. Könenkamp
Hahn-Meitner Institut Berlin, Glienicker Street 100, 14109 Berlin, Germany
(Received 9 August 1999)

Recent results on electron transport in nanoporous TiO_2 films with gas-filled, insulating pores are evaluated. Measurements on Pt/TiO_2 Schottky barrier structures indicate a barrier height of 1.7 eV, compatible with an electron affinity of 3.9 eV for the TiO_2 films. Below ~300 K, tunneling transport through the barrier occurs, resulting in barrier lowering effects. Carrier drift mobilities, recombination lifetimes and their dependence on injection level in TiO_2 are reported. It is found that the mobility-lifetime product is independent of injection level, while drift mobility and recombination lifetime change strongly with injection. All experimental findings are discussed in terms of two different transport models, one based on trap filling, the other on the screening of potential fluctuations. The trap filling model appears as the more plausible model. Comparison with recent experiments on nanoporous films in contact with electrolytes indicate that the transport and recombination mechanism is qualitatively similar for the two cases.

INTRODUCTION

Porous nanocrystalline semiconductors have attracted considerable interest in recent years due to their excellent performance in applications for gas sensing, catalysis, photovoltaics, light and laser emission, and electrochromism.[1–6] While several device applications have already been demonstrated, the schemes of electron propagation and a quantitative evaluation of the transport parameters have so far not been completely established. The present paper addresses this issue and evaluates experimental results of carrier transport in porous TiO_2 films, in which the pores are filled with an insulating medium, i.e., air or N_2. The samples are Schottky barrier diodes with the TiO_2 film sandwiched between an ohmic SnO_2 back contact and a metal top providing rectification. This simple device structure allows to obtain quantitative insight into the electronic properties of the material and the basic features of carrier transport. Our results show that the carrier mobility and recombination kinetics strongly depend on the trap occupation. These findings are explained in two alternative transport models, based on trap filling and electric screening of internal potential fluctuations. While both models describe the experimental data well, it is proposed that the potential fluctuations model is less likely to apply.

Porous TiO_2 films filled with a conducting medium, mainly electrolytes, have also attracted interest due to their use in highly efficient electrochemical solar cells.[6] In this application the pore surface is covered with an ultrathin organic dye-layer and contacted with an electrolytic solution which penetrates the pore structure. The experimental work indicates[7–10] that in this configuration the electrolyte screens any electric field within the porous structure and establishes diffusion conditions for the carrier propagation. Apart from the screening, the electrolyte is likely to affect the grain surface also by chemical effects, and may influence the electronic equilibrium within the grains by charge transfer from the electrolyte. Thus, while in these electrolytically contacted devices the TiO_2 material itself is quite similar to the material used here, it is not clear to what extent the transport behavior is comparable. The results will also be discussed with respect to transport models for films with conductive pores.

PREPARATION

The TiO_2 film preparation uses a sol-gel technique based on a TiO_2 collloid. The colloid is prepared from titanium isopropoxyde and isopropanol in water. For the peptization, nitric acid is added. Subsequent boiling induces the crystallization of TiO_2 particles and the evaporation of organic components.[11–13] Anatas crystallites with average diameter as small as ~10 Å can be prepared in this way. Crystallites with size below 1 μm are monocrystalline and have fairly compact shape.

Anatas TiO_2 films are prepared from these colloidal suspensions using a room temperature spin coating process.[11] After deposition the films are heated for several minutes at temperatures around 450 °C. Deposition and heating cycles are repeated until the desired film thickness is obtained. A final sintering step is applied at temperatures of ~650 °C and results in porous ceramic-type films consisting of 40–80 Å diameter anatas crystallites with a pore volume of ~50%. In films of several μm thickness the inner pore surface is typically a few hundred times larger than the plane projection.

The Schottky barrier structures are prepared on SnO_2 coated glass that provides the ohmic back contact to the TiO_2. Vacuum evaporated Pt dots of ~3 mm diam and a typical thickness of 150 Å establish the Schottky barrier contact on top of the films. Electron micrographs indicate that the Pt layer covers the top surface of the nanoporous film as a connected film. Pt penetration into the film is not observed and to a good approximation the contact geometry can be considered as planar.

PHOTOELECTRICAL CHARACTERIZATION

Figure 1(a) shows the current-voltage characteristics in these devices. The observed strong rectification clearly indicates that an efficient Schottky barrier is established. As discussed previously,[14] the current response to changes in the

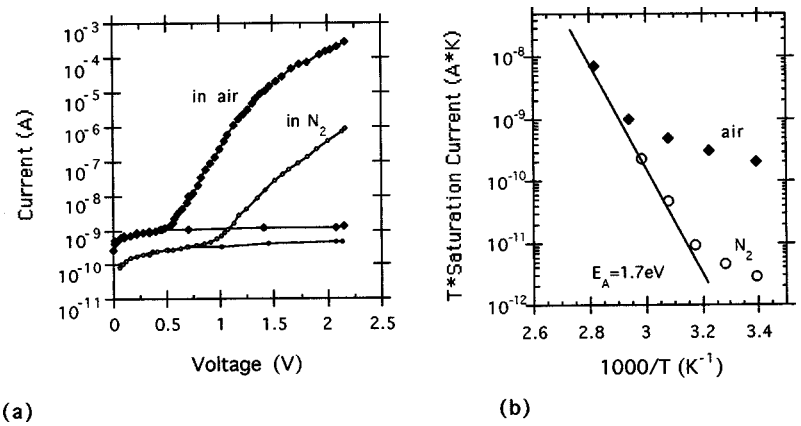

FIG. 1. (a) Current-voltage characteristics of SnO_2/TiO_2/Pt Schottky barrier samples. Solid data points were obtained in lab air ambient at standard conditions, open symbols refer to dry N_2 ambient. (b) Temperature dependence of the saturation current in air (solid symbols) and dried N_2 (open symbols). Towards higher T tunneling becomes less important and an activation energy of ~1.7 eV can be extracted.

applied potential is very slow, indicative of slow carrier transport and a slow trap filling process. For the measurements in Fig. 1(a) the voltage scan period is typically several minutes to ensure stationary current flow. The details of the I-V characteristics strongly depend on the gas ambient. This dependence is, of course, the basis for the gas sensing capabilities of the material. Fig. 1(a) shows the variation in the I-V curves for dried N_2 and lab air ambients. Although the differences in the electrical behavior are large, qualitative features of rectification, exponential forward currents, and low reverse currents are maintained. The observed differences can be explained in terms of charged surface states induced by the adsorption of O_2^-, O_2^{2-}, and H_2O.[15–17] Despite the magnitude of the effects shown in Fig. 1(a), it is thought that the qualitative conclusions drawn from the experiments remain valid for a wider variation of gaseous ambients, and, as will be pointed out below, even for electrolytic ambients. Quantitative aspects of the analysis presented in this paper, however, are restricted to films in lab air with I-V characteristic as in Fig. 1(a).

The data of Fig. 1 allow a basic description in terms of the Schottky barrier height, the electron affinity of the TiO_2, and some qualitative conclusion on the transport mechanism across the barrier. Below ~0.8 V forward bias the current is found to have only a small temperature-dependence, indicating that the transport is due to tunneling or a metallic leakage path. The current increase is exponential in the forward bias range, $\sim 0.8\,\mathrm{V} < V_F < 2\,\mathrm{V}$, and we attribute this behavior to transport across the Pt-Schottky barrier. For $V_F > 2\,\mathrm{V}$ one observes a nonexponential, superlinear current-voltage dependence, indicative of double injection from the two contacts. For the Schottky-barrier regime one expects the current to be given by

$$i = J_0\left[\exp\left(\frac{eV}{nkT}\right) - 1\right], \qquad (1)$$

where i is the current, J_0 is the reverse saturation current, V the applied voltage, n the diode quality factor, k Boltzmann's constant, and T the temperature. Typically, diode quality factors around $n \approx 2.5$ are observed. Extrapolation of the exponential region to zero voltage gives the saturation current, J_0, whose temperature dependence allows a determination of the barrer height, Φ. Due to the low-carrier mobilities in these nano-crystalline films, diffusion theory is applicable for the evaluation of the current-voltage curves. In the diffusion transport model the barrier height can be determined from the saturation current by using[18]

$$J_0 = \left\{\frac{q^2 D N_c}{kT}\left[\frac{q(V_{bi}-V)2ND}{\varepsilon}\right]^{1/2}\right\}\exp\left(-\frac{q\Phi}{kT}\right), \qquad (2)$$

where q is the electron charge, D is the diffusivity, N_C is the conduction band density of states, V_{bi} is the built-in potential, and N the donor density. At low temperatures tunneling through the barrier may set in, therefore the activated behavior predicted by Eq. (2) should be most pronounced at higher T. Figure 2(b) confirms this expectation, activated behavior is found only at elevated temperatures, while for lower T the data show a much weaker temperature dependence for both, N_2 and lab air ambients. In the high temperature regime one finds a barrier height of approximately 1.7 eV. In agreement with previous reports on this material[15] we attribute the differences mainly to water adsorption. Apparently, in the dry N_2 ambient, particularly after a moderate heat treatment, the grain surfaces have less water adsorbed, the material therefore exhibits more intrinsic electronic properties with a low conductivity and a Fermi-level near midgap. As a consequence, the barrier depletion region is wide and electron transport involves thermal activation across the barrier. In lab air there is partial adsorption of H_2O in the device, which results in an increased defect density,[15,16] a larger conductivity due to charge transfer and thus a narrower depletion region. The electron transport over the barrier then looses out

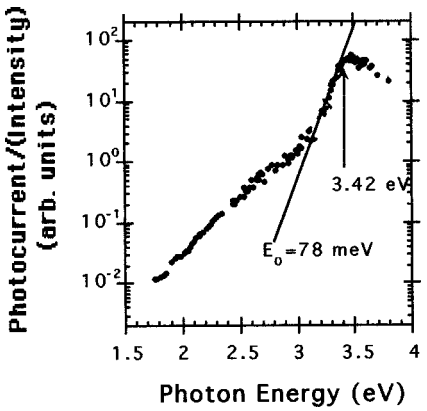

FIG. 2. Photocurrent response sprectrum of porous TiO_2 films showing two exponential tails with characteristic energies $E_0 = 78\,\mathrm{meV}$ and $E_1 = 200\,\mathrm{meV}$. The arrow indicates the band-gap energy.

against defect-assisted tunneling through the barrier with a much weaker temperature dependence.

TiO_2 belongs to a group of polar insulators which exhibit little or no Fermi-level pinning, and it is therefore possible to obtain an estimate for the electron affinity from barrier height measurements. Using 5.6 eV for the Pt work function[19] and 1.7 eV for the TiO_2/Pt barrier height, one obtains an electron affinity of ~3.9 eV for the nano-porous films. This value agrees well with estimates for porous films from electrochemical experiments and with results for anatas single crystals.[20]

Figure 2 shows the photocurrent spectrum of the Schottky barrier devices in reverse bias. The photocurrent is attributed to electron transport, since it is well-known that the hole mobilities in anatas TiO_2 are extremely small. The response in the region, $2<h\nu<3.3$ eV, gives clear evidence for the existence of localized states in the band-gap region. For energies between 3.1 and 3.3 eV the spectrum exhibits a steep exponential tail with a bandtail parameter, $E_0=78$ meV. At lower energies there is a broader tail, whose energy dependence is also exponential with a parameter, $E_1=200$ meV. This deep tail extends down to midgap energies. Since the photocurrent depends on the transition matrix element and the quantum generation efficiency, the data cannot easily be transformed into a density of states or an absorption coefficient. Some qualitative conclusions can, however, be drawn from Fig. 2. Photoconductance tails, as observed here for nano-porous TiO_2, are most pronounced in amorphous and glassy materials,[21,22] but can also be observed in high-quality single crystals.[23] They are a sensitive indicator of structural or thermal disorder effects. In glasses and amorphous semiconductors the tails are of the order of 100 meV while in crystals, they are much narrower, typically only a few meV. In TiO_2 anatas and rutile crystals the tail parameter is ~35 meV as determined by Tang.[24] The experimental work in Ref. 24 suggests that the tails result from a disorder-induced superposition of exciton lines. In the crystals the transition between the band and the tail region lies at $E_G=3.42$ eV, which agrees with the value found in our films. It is likely that structural disorder on the grain surfaces and interfaces gives rise to the enhanced broadening in the nanoporous material. Since the tail states are localized, the depth of the bandtail has a profound effect on the electronic transport properties. From extensive work on glassy and amorphous semiconductors it is known that a transition to dispersive transport occurs as the tail parameter becomes larger than the measurement temperature. With $E_0\approx 80$ meV one may therefore expect some similarities in the transport properties between these nanocrystalline films and amorphous materials.

TRANSPORT EXPERIMENTS

While in crystalline TiO_2 electron mobilities around 15 cm^2/Vs and hole mobilities in the 10^{-3} cm^2/Vs range[25] have been measured, our results and more recent investigations[26] indicate that in porous films the electron drift mobilities are below 10^{-3} cm^2/Vs. Hole drift mobilities in nanoporous TiO_2 have so far not been reported and are likely to be even smaller. Band structure calculations indicate that the density of states in the conduction band is of the order of $N_0\approx 10^{22}$ cm^{-3} eV^{-1}.[27] When the transition between extended band states and localized tail states occurs near the band edge energy, as is indicated by the photoconductance spectra of Fig. 2, the bandtails would comprise approximately 10^{21} cm^{-3} states. Starting from these basic considerations and experimental results published by us earlier,[14] we will set up a simple model for the description of carrier transport in the nanoporous films. The experimental results were obtained from junction recovery experiments under steady-state forward bias conditions. The method and its application to TiO_2 have been discussed in detail in.[14,28–30] For the interpretation of these results a brief outline of the experiment will be given next: The Schottky diodes are first biased in forward direction for sufficiently long times to obtain steady-state conditions. Under the forward current flow excess electrons and holes are injected into the device where they recombine. Under appropriate conditions[30] the forward current density is given simply by $i=Q_0/\tau$, where Q_0 is the excess injected charge and τ the recombination lifetime of the injected carriers. Q_0 is measured by a fast switching into reverse bias and an integration over the current transient, which results from the depletion of the diode. Figure 3(a) shows these extraction transients on a logarithmic scale. The solid line indicates the contribution due to the geometric capacitance, which can be determined independently and must be subtracted to obtain Q_0. The transients exhibit non-exponential time dependence typical for dispersive transport conditions. When the extraction of the excess charge is faster than the recombination process, practically all excess carriers can be collected. When the applied reverse voltage is only

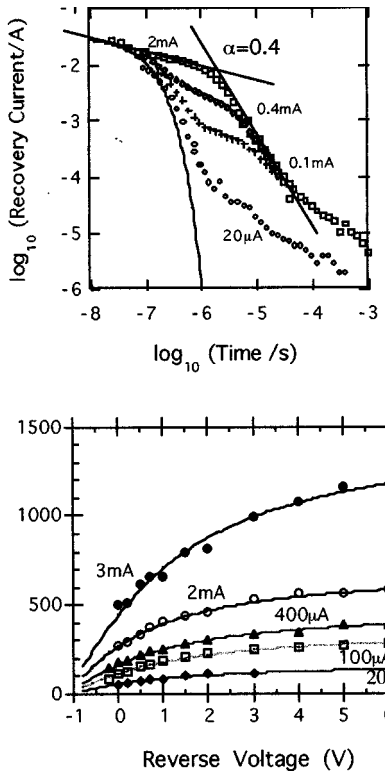

FIG. 3. (a) Recovery transients obtained on TiO_2/Pt Schottky barrier devices. The diode is switched from steady-state forward bias into reverse bias, the reverse current transient is plotted. (b) Recovered charge vs. reverse voltage determined by integration over the transients. The solid lines are least-square fits to Eq. (3), for the determination of the $\mu\tau$ product (Ref. 14).

weak, part of the excess charge recombines during extraction. A simple analysis[28] predicts the voltage dependence of extracted charge, Q, to be given by,

$$Q = Q_0 \frac{\mu\tau V}{L^2}\left[1 - \exp\left(-\frac{L^2}{\mu\tau V}\right)\right] \tag{3}$$

with μ the drift mobility, τ the recombination time, L the device thickness, and V the reverse voltage. By measuring this dependence Fig. 3(b) one determines the mobility-lifetime product, $\mu\tau$, and then calculates the drift-mobility, μ. Figure 4 summarizes the experimental results in terms of these transport parameters. The evaluation shows that the $\mu\tau$ product is approximately constant at $\sim 10^{-10}\,\mathrm{cm}^2/\mathrm{V}$, while the recombination lifetime and drift mobility strongly depend on injection level. Typical values for the drift mobility are in the range, $10^{-7} < \mu < 4\times 10^{-4}\,\mathrm{cm}^2/\mathrm{Vs}$.

ANALYSIS AND TRANSPORT MODELS

Next, we discuss two alternative models to explain these findings, one explanation involving trap filling as the underling mechanism, while the other is based on the screening of internal potential fluctuations.

TRAP-FILLING MODEL

The trap-filling model assumes that in forward bias the trap states are filled with excess carriers, and multiple trapping as the predominant transport mode. Tunneling as a recombination or transport mechanism is neglected.[31,32] The extraction kinetics is explained in terms of a transport process where the limiting step is the thermal emission from localized states.[14,28] The trap states relevant for the transport are the bandtail states and have a distribution given by, $N(E) = N_0 \exp(-E/E_{0c})$ with N_0 the density of states at the band edge and E_{0c} the conduction bandtail parameter. The band edge is at $E=0$ and the bandtail lies at negative energies. For a description of the experimental data it is useful to distinguish between shallow and deep trap states. For the shallow states thermal emission to the band edge is faster than recombination and the occupation of the shallow states is therefore a thermal equilibrium distribution. For the deep states recombination is more likely than thermal emission and their occupation is therefore determined by the recombination kinetics. The transition energy between the two occupation functions is the trap quasi-Fermi-level, E_{FT}, which depends on the injection rate, i.e., forward current. For forward bias the carrier distribution in the shallow states of the tail is given by,

$$n_s(E) = \gamma N_c \exp(E_{FT}/kT)\exp\left[(\alpha - 1)\frac{E}{kT}\right] \tag{4}$$

while the deep carrier distribution in the tail is given by,[33]

$$n_d(E) = \gamma N(E) = \gamma N_0 \exp\left(\frac{E}{E_{0c}}\right), \tag{5}$$

where $\alpha = kT/E_{oc}$ and γ is the occupation factor of the deep traps. In the extraction process the rate limiting step for the collection of these carriers is thermal emission. A trap at energy E has an average emission time, $t = \nu^{-1}\exp(E/kT)$, where ν is an attempt-to-escape frequency, such that carriers from deeper traps are depleted at later times than the more shallow carriers. During the emission time

$$t = \nu^{-1}\exp(E/kT), \tag{6}$$

a slice of trapped carriers kT wide at E is emitted and collected. This suggests to define a thermalization edge for the depletion process, $E(t) = kT\ln(\nu t)$, which separates the emitting traps from the deeper ones with frozen-in carriers. Initially, when the thermalization edge is above E_{FT}, the emission current is given by

$$i(t) \propto \frac{dn_s[E(t)]}{dt}\alpha(\nu t)^{-\alpha} \tag{7}$$

while for later times, when the thermalization edge is below E_{FT}, the emission current is given by

$$i(t) \propto \frac{dn_d[E(t)]}{dt} \propto (\nu t)^{->a-1}. \tag{8}$$

These two time regimes are clearly apparent in the experimental data of Fig. 3(a), and an analysis of the data shows that for both regimes, $\alpha = 0.4 \pm 15\%$. It follows that the parameter for the conduction band tail is, $E_{0c} = 62 \pm 10\,\mathrm{meV}$. This value is consistent with the Urbach tail of Fig. 2, since both, valence and conduction band tails contribute to the Urbach tail, and E_0 should therefore be larger than the conduction bandtail parameter alone. Since in the deep states the carrier distribution is simply given by $\gamma N(E)$, the model also predicts that towards long times the recovery transients should fall on a common curve. A comparison to the experimental results shows that this is borne out by the data. Only the transient obtained for a forward current of 20 μA departs from this expectation, but it may be expected that the approach will occur at later times, since E_{FT} for $i_F = 20\,\mu\mathrm{A}$ lies in very deep states.

The model gives a straightforward explanation to the current-dependent mobility behavior. The drift mobility is defined as an average taken over all injected excess carriers and is therefore given by, $\mu = \mu_0 n_f / n_{\mathrm{tot}}$. When there is no additional recombination path and the recombination process only involves transport in band states (as assumed), the recombination time is given by $\tau = \tau_0 n_{\mathrm{tot}}/n$, where τ_0 is the free carrier recombination time.[32] It is noted that under these conditions $\mu\tau$ is constant, as observed in Fig. 3. Since the ratio n_f/n_{tot} changes with the filling of trap states, it is clear that the mobility and recombination time depend on the injection level. For the exponential bandtail distribution, it can be shown,[31,32] that the ratio between the free carrier density, n_f, and the total injected carrier density, n_{tot}, is given by

$$\frac{n_f}{n_{\mathrm{tot}}} \approx \left(\frac{\alpha}{2-\alpha}\right)^{1/a}\left(\frac{n_{\mathrm{tot}}}{kTN_c}\right)^{(1-\alpha)/\alpha}. \tag{9}$$

In our case n_{tot} is given by the stored charge Q, therefore the consistency of the model can be checked with the experimental data, i.e., Eq. (7) offers a second way for the determination of α. The experimental data indicate $\tau \sim i_{F^{-0.6}}$ and $Q \sim i_{F^{0.4}}$. It follows that $\tau \sim Q^{-1.5}$ and therefore from Eq. (9), $\alpha = 0.4$, which is in good agreement with the kinetic results.

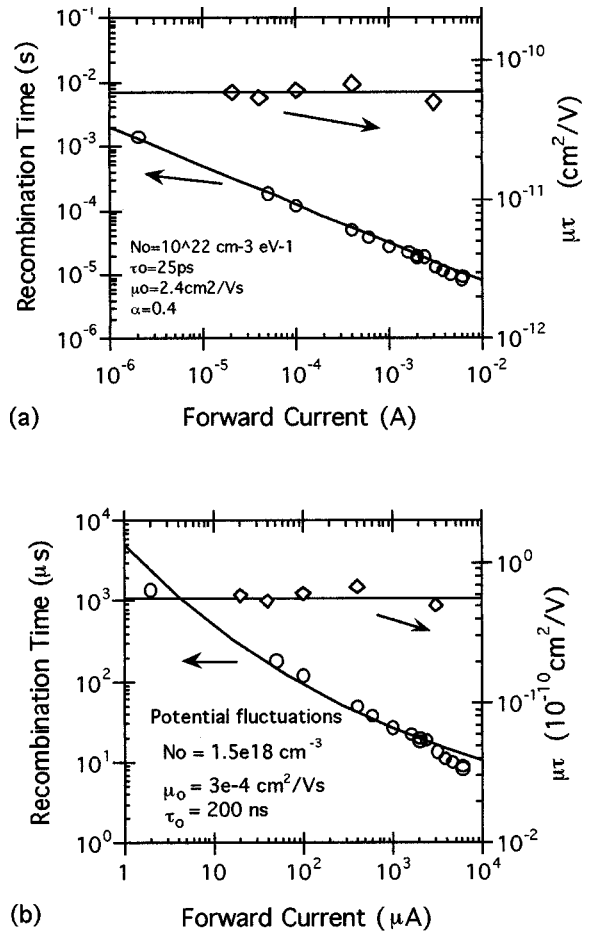

FIG. 4. (a) Summary of experimental results from junction-recovery measurements (open symbols), and numerical fit to the data on the basis of the multiple trapping model. The main model parameters are given in the inset. (b) Same as (a) for the potential fluctuations model.

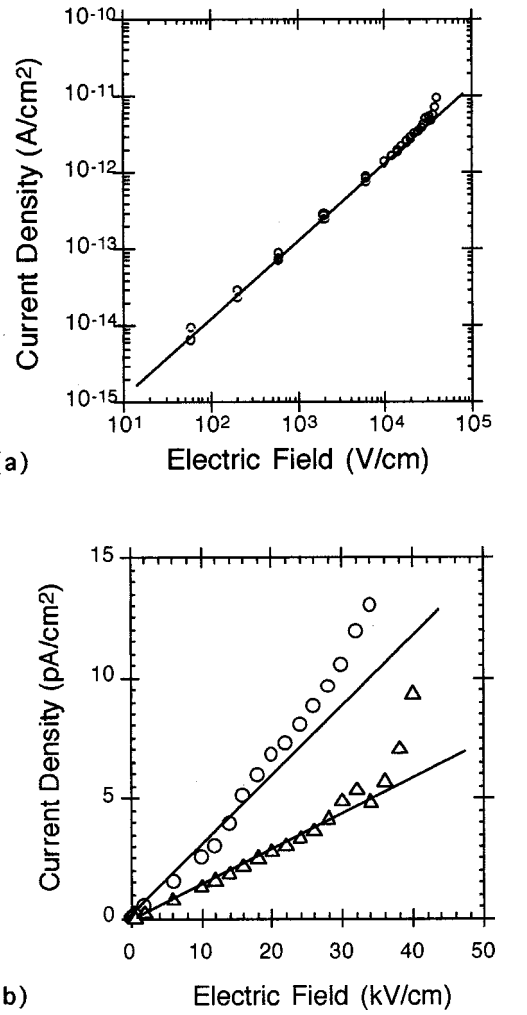

FIG. 5. (a) Logarithmic plot of the current-voltage dependence for coplanar strip contacts, strip separation 500 μm, strip length 10 mm, film thickness 5 μm. (b) Linear plot of the current-voltage dependence in the 10^4 V/cm range for two samples, showing superlinear behavior.

The combination of all results allows a nearly complete determination of the model parameters. The only remaining adjustable parameter is N_0. As mentioned above, however, from band-structure calculations N_0 can be estimated to be of the order of $10^{22}\,\mathrm{cm}^{-3}$. The data in Fig. 4 were therefore fitted by taking $N_c = 10^{22}\,\mathrm{cm}^{-3}$. The obtained results for the free carrier mobility, μ_0, the free carrier recombination time, τ_0, and the band tail parameter E_{0c} based on this assumption are shown in Table I. The solid lines in Fig. 5(a) result from this set of input parameters. It is seen that the experimental results can satisfactorily be described. The free carrier mobility of 2.4 cm^2/Vs is of the same magnitude as in TiO_2.[25] This suggests that the nanosize grains are of good crystalline quality. The free carrier recombination time, τ_o, is found to be in the picosecond range, indicating fast capture of free carriers into the trap states.

TABLE I. Fitted parameters from trap filling model.

Band tail parameter, E_{0c}:	62 meV
Free carrier mobility, μ_0:	2.4 cm^2/Vs
Free carrier recombination time, τ_0:	25 ps
DOS at mobility edge, N_c:	$10^{22}\,\mathrm{cm}^{-3}\,\mathrm{eV}^{-1}$

POTENTIAL FLUCTUATIONS

The observed mobility changes can also be explained in terms of a different model, based on the screening of potential fluctuations by excess carriers. Statistical arguments, first proposed by Jäckle,[34] account for the occurrence of potential fluctuations as a result of localized charges associated with point defects and impurities. Potential fluctuations are therefore of particular relevance in compensated materials,[35,36] since these have low thermal carrier densities and a large number of charged impurities. For the porous films used here compensation effects may be relevant since O vacancies in the bulk give rise to positively charged centers, while surface-adsorbed species are known to act predominantly as electron traps, and do thus exert a compensating influence.

In the following, Jäckle's model will be applied for an interpretation of the junction-recovery results. For a given charged impurity concentration, N, and a mobile carrier concentration, n, the mean amplitude of the potential fluctuations is given by[34]

$$\Delta = 1.28(q/\varepsilon\varepsilon_0)N^{1/3}(N/n)^{1/3} \tag{10}$$

TABLE II. Fitted parameters for potential fluctuations model.

Charge defect density, N:	$1.5\times10^{18}\,\mathrm{cm}^{-3}\,\mathrm{eV}^{-1}$
Free carrier mobility, μ_0:	$3\times10^{-4}\,\mathrm{cm}^2/\mathrm{Vs}$
Free carrier recombination time, τ_0:	200 ns
Dielectric constant, ε:	30

and the screening length for the potential fluctuations is

$$\lambda = 0.28 n^{-1/3} (N/n)^{1/3}, \tag{11}$$

where $\varepsilon\varepsilon_0$ is the permittivity of the porous TiO_2, and $\varepsilon \approx 30$ was used. Thus both, the average amplitude and the spatial extension of the potential fluctuations depend on the carrier density, n. Since carriers trapped at bandtail energies have emission times that are short compared to the times, that are necessary to establish stationary currents, n has to comprise the carriers trapped in the bandtails and free carriers in the band states. Thus for the screening, all of the recovered charge, n_{tot}, has to be considered. The model assumes that carrier transport and recombination involve thermal activation across barriers which are approximately half the size of the average potential fluctuations. The drift mobility and recombination time will then depend on an effective barrier height, $\Delta/2$, as

$$\mu = \mu_0 \exp(-\Delta/2kT) \tag{12}$$

and

$$\tau = \tau_0 \exp(\Delta/2kT). \tag{13}$$

The barrier height $\Delta/2$ thus takes a similar role as the trap depth in the multiple trapping model. The physical difference between the two models lies in the mechanism of barrier lowering. In the trap-filling model, the average trap depth decreases due to the filling process. This results in a changed ratio of free and trapped carriers, which in turn leads to an increased drift mobility for increased injection. Since the recombination is transport limited, the recombination time decreases in reciprocal fashion. In the potential fluctuation model, the barrier lowering results from screening by the injected carriers, which also leads to an increase of the drift mobility at higher injection levels, and a lower recombination time.

Since n, μ, and τ are experimentally accessible, the problem is well-defined. The solid lines in Fig. 5(b) show an evaluation of the experimental data in terms of the potential fluctuation model, taking $\varepsilon = 30$ for the porous TiO_2. The available data give $\mu_0 = 3\times10^{-4}\,\mathrm{cm}^2/\mathrm{Vs}$, $\tau_0 = 200\,\mathrm{ns}$, and $N = 1.5\times10^{18}\,\mathrm{cm}^{-3}$. The barrier heights lie in the range, $100\,\mathrm{meV} < \Delta < 400\,\mathrm{meV}$, typical screening lengths are between 100 Å and 1000 Å, and typical electric field strengths due to the potential fluctuations are several 10^4 V/cm. Figure 5(b) shows that the experimental results are well reproduced by the model. Since potential fluctuations are also quite consistent with the exponential tailing of the band edge,[21,36] they need to be considered for the transport in nanoporous TiO_2. The model parameters are summarized in Table II.

Probably the most straightforward method to obtain additional evidence for their existence is from the current-voltage behavior under ohmic contact conditions, using, for example, a planar contact arrangement. One would expect that the superposition of an external field results in a lowering of the average barrier height in the direction of the current. The field induced barrier lowering would result in an increased drift mobility and thus a superlinear current-voltage dependence. Figure (5) shows I-V plots covering electric fields up to several 10^4 V/cm. The data were taken in the dark, where the field strength due to potential fluctuations is smallest. Part (a) of the figure indicates that below 10^4 V/cm the dependence is accurately ohmic, while above 10^4 V/cm there is a clear superlinear rise in the current, which—unfortunately—soon leads to irreversible breakdown in the film. The superlinear regime is shown in a linear plot in part (b). It is noticed that the superlinearity is accompanied by small irreproducible variations in the current density, which lead to scatter in the data. These temporal variations may be a pre-breakdown phenomenon. While the superlinear behavior is compatible with the existence of potential fluctuations, there are also several other effects, such as space charge injection, dielectric breakdown and filament forming effects in the porous network, which can all give rise to superlinear currents. It would be worthwhile to study this behavior in more detail, but it will certainly remain a difficult task to use these data to discriminate between different transport models. At present it can only be stated that unequivocal experimental evidence against potential fluctuations in the porous TiO_2 could not be established. It is noted, however, that the charged defect density N derived from the potential fluctuation model is surprisingly large. Neither optical nor any other experiments give evidence for the presence of such large deep defect densities in the nano-porous films. It is also difficult to give a straightforward physical explanation to the low free carrier mobility suggested by the model, and the comparably large free carrier recombination time. In fact, decay kinetics much shorter than 200 ns have been observed in time-resolved photoconductance measurements, but these fast decays have been attributed to trapping in shallow states rather than recombination in deep centers.[11]

DISCUSSION AND CONCLUSION

We have carried out an analysis of transport experiments on nanoporous TiO_2 films with gas filled pores. Schottky-diode structures in lab air ambient were used for these experiments. These are characterized by a barrier height of 1.7 eV at high temperatures. At room temperature the Schottky contact still exhibits excellent rectification, but the effective barrier height is lowered, likely due to tunneling conduction through the tip of the barrier. It was shown that junction-recovery results allow a quantitative description of carrier transport and recombination kinetics in these TiO_2 films. The results relate to steady-state injection conditions. These conditions are different from those of time-of-flight experiments, which are non-steady-state conditions and usually relate to depleted diodes. Here it was shown that a satisfactory description to the experimental data can be given either in terms of a trap-filling mechanism or on the basis of a potential-fluctuations model.

From current-voltage measurements the existence of potential fluctuations could not be excluded. The model pre-

dicts, however, the density of deep charged states to be in excess of $10^{18}\,cm^{-3}$, which appears excessively high. We therefore prefer the trap-filling model. This model suggests the following picture for the carrier transport in the nanocrystalline films: Similar to the case of amorphous semiconductors, the carrier transport in the nanoporous films is dispersive,[11,37] involving a trap filling mechanism in an approximately exponential bandtail. The values for the free carrier mobility and recombination lifetimetimes are 2.4 cm^2/Vs and 25 ps, respectively. It appears that the transport within the grains is fairly efficient, and it is therefore suggested that the trapping occurs in interface and surface states. For a grain diameter of 100 Å or less, one finds that the surface state density becomes comparable to the observed bandtail density of states. Only for the highest injection levels the mobilities are compatible with the electron diffusion constants in films whose pores are filled with electrolytes.[7,26] This finding may partly be due to differences in grain size and constituency between the different sample sets. Beyond this more trivial explanation it appears possible, however, that the charge transfer at the electrolyte/TiO_2 contact induces trap filling in the TiO_2, and thereby improves the transport behavior. The electrolytic contact may also provide electrochemical surface passivation, and thereby reduce the surface state density as a whole. Recent work on electrolytically contacted films finds the diffusion length not to be dependent on the illumination level, while the diffusion constant and the recombination time depend on illumination level.[38] Since the Einstein relation, which relates diffusion and drift parameters, is valid also for the case of dispersive transport conditions,[39] it is possible to compare the diffusion and drift parameters for the two sets of films. The analysis shows that the diffusion results agree well with $\mu \sim i^{\alpha}$, $t \sim i^{-\alpha}$ and $\mu\tau \sim$ constant with only marginally different values for the power exponent. This finding strongly suggests that the transport model derived in this paper for films in dry ambients may also be applicable in films with conducting pores. The main difference between the two types of samples would then be the numerical value of the relevant parameters, μ_0, τ_0, and α. Further confirmation of this hypothesis is obtained from a recent paper by Nelson[10] who applies a random-walk model based on trapping for the description of transport in electrolytically contacted TiO_2. This congruence of results suggests that the propagation kinetics in the two types of films is qualitatively similar, involving in both cases bandtail states and transport-limited recombination conditions. Since E_0, E_{0c}, and α are the parameters that describe the trapping distribution, these may be considered the relevant quality parameters for a comparison of different sets of films. While the presented transport and recombination model is able to describe the experimental findings, it treats the porous structure as an effective medium, and does not yet account for details in the topology of the structure. This approach appears justified as long as the connectivity among grains is sufficiently large, as in indicated by electron microscope results on our films. The approach may, however, become problematic in the limit that the connectivity among grains is small, and percolation becomes the rate-limiting transport step. For this case it may be necessary to employ a topological model for the carrier propagation.

[1] H. Weller, Angew. Chem. Int. Ed. Engl. **32**, 41 (1993).
[2] L. N. Lewis, Chem. Rev. **93**, 2693 (1993).
[3] A. Henglein, J. Phys. Chem. **97**, 5457 (1993).
[4] E. Pelizetti, C. Minero, E. Praauro and M. Vincenti, *Proceedings of the International Conference on Photochemical and Photoelectrochemical Conversion and Storage of Solar Energy 1992* (International Academic Publishers, Bejing, 1993), p. 217.
[5] C. Bechinger, E. Wirth, and P. Leiderer, Appl. Phys. Lett. **68**, 2843 (1996).
[6] B. O'Regan and M. Grätzel, Nature (London) **353**, 737 (1991).
[7] P. E. de Jongh and D. Vanmaekelbergh, Phys. Rev. Lett. **77**, 3427 (1996).
[8] A. Zaban, A. Meier, and B. A. Gregg, J. Phys. Chem. B **101**, 7985 (1997).
[9] A. Solbrand, H. Lindström, H. Rensmo, A. Hagfeldt, and S. Lindquist, J. Phys. Chem. B **101**, 2514 (1997).
[10] J. Nelson, Phys. Rev. B **59**, 15 374 (1999).
[11] R. Könenkamp, A. Wahi, and P. Hoyer, J. Phys. Chem. **97**, 7328 (1993).
[12] B. O'Regan, J. Moser, M. A. Anderson, and M. Grätzel, J. Phys. Chem. **94**, 8720 (1990).
[13] D. W. Bahnemann, C. Kormann, and M. R. Hoffmann, J. Phys. Chem. **91**, 3789 (1987).
[14] R. Könenkamp and R. Henninger, Appl. Phys. A: Solids Surf. **58**, 87 (1994).
[15] T. Wolfram, R. Hurst, and F. J. Morin, Phys. Rev. B **15**, 1151 (1977).
[16] V. Henrich and R. L. Kurtz, Phys. Rev. B **23**, 6280 (1981).
[17] R. L. Kurtz, R. Stockbauer, T. E. Madey, E. Roman, and J. L. de Segovia, Surf. Sci. **218**, 178 (1989).
[18] S. M. Sze, *Physics of Semiconductor Devices* (Wiley, New York, 1981).
[19] H. B. Michelson, IBM J. Res. Dev. **22**, 72 (1978).
[20] G. Rothenburger, D. Fitzmaurice, and M. Grätzel, J. Phys. Chem. **96**, 5983 (1992).
[21] N. F. Mott, and E. A. Davis, *Electronic Processes in Non-Crystalline Materials* (Clarendon, Oxford, 1979).
[22] G. D. Cody, in *Semiconductors and Semimetals*, edited by J. I. Pankove (Academic, New York, 1984), Vol. 21B, Chap. 2.
[23] M. Beaudoin, A. J. G. DeVries, S. R. Johnson, H. Laman, and T. Tiedje, Appl. Phys. Lett. **70**, 3540 (1997).
[24] H. Tang, Ph.D. thesis, Physics Department, Ecole Polytechnique Federale de Lausanne, 1995.
[25] L. Forro, O. Chauvet, D. Emin, L. Zuiroli, H. Berger, and F. Levy, J. Appl. Phys. **75**, 633 (1994).
[26] T. Dittrich, E. A. Lebedev, and J. Weidmann, Phys. Status Solidi A **165**, R5 (1998).
[27] F. M. F. de Groot, J. Faber, J. J. M. Michiels, M. T. Czyzyk, M. Abate, and J. C. Fuggle, Phys. Rev. B **48**, 2074 (1993).
[28] R. Könenkamp, A. M. Hermann, and A. Madan, Appl. Phys. Lett. **46**, 405 (1985).
[29] R. Könenkamp, A. M. Hermann, and A. Madan, J. Non-Cryst. Solids **66**, 249 (1984).
[30] A. Hoffmann and K. Schuster, Solid-State Electron. **7**, 717 (1969).

[31] T. Tiedje and A. Rose, Solid State Commun. **37**, 49 (1980).
[32] J. Orenstein and M. Kastner, Phys. Rev. Lett. **46**, 1421 (1981).
[33] A. Rose, *Photoconductivity and Allied Problems* (R. E. Krieger Publications, Huntington, New York, 1978).
[34] J. Jäckle, Philos. Mag. B **41**, 681 (1980).
[35] H. Overhof, J. Non-Cryst. Solids **66**, 261 (1984).
[36] D. E. Theodorou and H. J. Queisser, Phys. Rev. Lett. **58**, 1992 (1987); S. John, C. Soukoulis, M. H. Cohen, and E. N. Economou, *ibid.* **57**, 1777 (1986).
[37] K. Schwarzburg and F. Willig, Appl. Phys. Lett. **58**, 2520 (1991).
[38] L. M. Peters, G. Franco, E. A. Ponomarev, N. J. Shaw, K. G. U. Wijayantha, and L. Yuan, *Fourth International Symposium on New Trends in Photoelectrochemistry* (Sophia Antipolis, France, 1999), Book of Abstracts.
[39] Q. Gu, E. A. Schiff, S. Grebner, F. Wang, and R. Schwarz, Phys. Rev. Lett. **76**, 3196 (1996).